

Strength distribution of planar local load sharing bundles

C. N. Irfan Habeeb* and Sivasambu Mahesh†

Department of Aerospace Engineering, Indian Institute of Technology Madras, Chennai 600 036. India.

Monte-Carlo simulations and probabilistic modelling are employed to understand the strength distribution of a planar bundle of local load sharing fibres. The fibres are distributed randomly within a unit square according to a Poisson process, and the fibre strengths are Weibull distributed with exponent ρ . Monte-Carlo failure simulations of bundles comprised of up to 10^5 fibres suggests that the bundle strength distribution obeys weakest-link scaling for all ρ . Also, a probabilistic model of the weakest-link event is proposed. This model introduces a failure event at a size scale between that of the fibre and that of the bundle, whose failure statistics follows that of equal load sharing bundles. The weakest-link event is modelled as the growth of a tight cluster of these equal load sharing bundles. The size of the equal load sharing bundles increases with decreasing ρ . The simulated bundle strength distributions and those predicted by the model are compared, and excellent agreement is obtained.

I. INTRODUCTION

I.1. Background

A bundle of long parallel fibres loaded in uniaxial tension along the fibre direction, besides representing the actual arrangement of phases in unidirectional fibre composites, also represents an idealised model of many heterogeneous materials. In these materials, randomness in the microstructural properties leads to random bundle strength. In the specific case of fibre composites, fibre strength, inter-fibre spacing, matrix strength, and fibre/matrix interface strength may be randomly distributed. It is important, both from theoretical and technological perspectives, to understand the interconnection between the probability distribution of microstructural properties and the bundle strength distribution. The past two decades have witnessed vigorous efforts toward understanding this interconnection, as summarised in the recent review articles by Alava et al. [1], and Pradhan et al. [2].

Amongst the class of bundle strength problems, the ‘bundle of threads’ or ‘equal load sharing bundle’ model has the simplest load sharing rule. In the equal load sharing (ELS) model of an n fibre bundle, of which r are broken, the remaining $n - r$ intact fibres are equally overloaded regardless of their proximity to the broken fibres. The stress concentration on the $n - r$ intact fibres is given by

$$K^{\text{ELS}} = n/(n - r). \quad (1)$$

Let ℓ denote the load per fibre, so that the total load applied to the bundle is $n\ell$. Let the strength of a single fibre be characterised by the cumulative distribution function $F(\ell)$. A pioneering result, due to Daniels [3] states that as $n \rightarrow \infty$, the ELS bundle strength $G_n^{\text{ELS}}(\ell)$ will be Gaussian distributed:

$$\lim_{n \rightarrow \infty} G_n^{\text{ELS}}(\ell) = \Phi((\ell - \mu)/s_n), \quad (2)$$

with mean

$$\mu = \ell_\tau(1 - F(\ell_\tau)), \quad (3)$$

and variance

$$s_n^2 = \ell_\tau^2 F(\ell_\tau)(1 - F(\ell_\tau))/n. \quad (4)$$

ℓ_τ denotes the value of ℓ at which $\ell(1 - F(\ell))$ maximises.

The ELS rule, Eq. (1), is a poor model of the actual load sharing when fibres are embedded in a continuous matrix phase. In this case, most of the load dropped by a broken fibre will be distributed amongst its proximate fibre neighbours. A model wherein the matrix only transmits shear stresses from broken fibres to their nearby intact fibres was proposed by Hedgepeth [4] for a one dimensional array of fibres embedded in matrix, and by Hedgepeth and Van Dyke [5] for a square lattice fibre arrangement. For a one-dimensional array, Hedgepeth’s [4] model predicts that the two neighbouring intact fibres surrounding a broken fibre carry a stress concentration of $\frac{2}{3}$, i.e., together they carry $\frac{2}{3}$ of the load dropped by the broken fibre. More distant fibres carry the remaining $\frac{1}{3}$ load dropped by the broken fibre. While realistic, the determination of stress concentration on intact fibres using the Hedgepeth [4] or Hedgepeth and Van Dyke [5] models is computationally tedious for model composites with more than a few thousand fibre breaks [6, 7].

The local load sharing (LLS) rule due to Harlow and Phoenix [8] represents a much simpler rule for load transfer from broken to intact fibres in a partially failed bundle. In the LLS rule, using a pre-defined distance norm, the intact fibres nearest each broken fibre are identified [8–11]. The load dropped by the broken fibre is then divided equally amongst the nearest intact fibres. The LLS rule results in greater overloading of the nearest neighbours of a broken fibre than the Hedgepeth model [4, 5], and no overloading at all of farther fibres. LLS overloads are thus more severe than those in Hedgepeth’s load sharing.

The interconnection between the strength distribution of the individual fibres and LLS bundle strength is more complex than that in an ELS bundle [1]. A important insight into this connection, due to Harlow and Phoenix [8],

* ae10b041@smail.iitm.ac.in

† Corresponding author: smahesh@iitm.ac.in

states that if $G_n^{\text{LLS}}(\ell)$ denotes the probability distribution function of an LLS bundle of n fibres, there exists a function $W(\ell)$ independent of n such that:

$$G_n^{\text{LLS}}(\ell) = 1 - (1 - W(\ell))^n. \quad (5)$$

Harlow and Phoenix termed $W(\ell)$ as the weakest-link strength distribution, and deduced strength scaling with bundle size on the basis of Eq. (5). They also gave an analytical expression for $W(\ell)$, based on a probabilistic model of sequential fibre breakage. In this model, successive breaks are assumed to occur under the stress overload produced by foregoing fibre breaks. Thus, event begins with the failure of one fibre, anywhere in the LLS bundle. The LLS overload on the neighbouring fibres leads to the failure of at least one of them, and subsequent overload on the neighbours of the pair of breaks. This process is assumed to continue, until the failure of the entire bundle. Because failure of successive fibre occurs under the influence of overload from the previously broken fibres, a cluster growth like failure mode is envisaged in this model. Smith [12] provided a mathematical proof of the existence of the weakest-link distribution using extreme-value probability theory, in the limit of $n \rightarrow \infty$ and in the limit of the scatter in the random fibre strength approaching zero. He also pioneered the use of Monte-Carlo simulations of bundle failure to obtain empirical bundle strength distributions. He showed good agreement between the probabilistic model for $W(\ell)$ and that obtained from the empirical distribution for small, but finite scatter of the fibre strengths. These arguments were later extended to a two-dimensional bundle wherein the fibres were arranged at the nodes of a hexagonal lattice by Smith et al. [10].

Ibnabdeljalil and Curtin [13] obtained the empirical distributions obtained from Monte-Carlo simulations performed in a three-dimensional elastic load sharing bundle of fibres. They found that there exists a bundle size n_c , such that the strength distribution of the elastic load sharing bundle weak-linked to n_c matches that of a global load sharing bundle of the same size. Similarly, in a planar bundle also with elastic load sharing, Curtin [14] considered weak-linking the bundle strength distribution $G_\gamma(\ell)$ to a critical sub-bundle size, n_c :

$$W^{n_c}(\ell) = 1 - (1 - G_\gamma(\ell))^{n_c/\gamma}. \quad (6)$$

He found that there exists a critical size, n_c for which the distribution $W^{n_c}(\ell)$ is Gaussian. Moreover, he found that the Gaussian distribution follows Eq. (2):

$$W^{n_c}(\ell) = \Phi((\ell - \mu^*)/s_{n_c}). \quad (7)$$

Here, n_c depends only on the fibre strength variability, but not on ℓ or γ . The mean strength, μ^* , in Eq. (7) differs from that given by Eq. (3). Curtin [14] was the first to connect the bundle strength distribution to that of ELS sub-bundles.

Let the fibre strengths L obey the Weibull distribution [15]:

$$F(\ell) = \Pr\{L \leq \ell\} = 1 - \exp(-\ell^\rho), \quad (8)$$

where ρ is termed the Weibull exponent. For this distribution, the mean strength μ_F and variance s_F^2 are given by

$$\begin{aligned} \mu_F &= \Gamma(1 + 1/\rho), \text{ and} \\ s_F^2 &= \Gamma(1 + 2/\rho) - \Gamma^2(1 + 1/\rho), \end{aligned} \quad (9)$$

respectively, where $\Gamma(t) = \int_0^\infty x^{t-1} e^{-x} dx$ [16]. The limit of low scatter in fibre strengths corresponds to $s_F^2 \downarrow 0$, which occurs when $\rho \rightarrow \infty$. In this limit, the sequence of fibre breaks in an LLS bundle is dictated by the LLS overloads, and successive breaks tend to form predominantly near pre-existing breaks, as noted above. However, as ρ decreases, and s_F^2 increases, the probability of occurrence of a fibre strong enough to withstand the overload imposed upon it by a neighbouring break also increases. This causes a break down of the cluster growth like failure mode at lower ρ . Breaks tend to be dispersed throughout the bundle domain, and at small ρ , the pattern of breakage in LLS bundles resembles that in an ELS bundle, where fibre locations are immaterial to the sequence of fibre breakage. Also, while the cluster growth like mode involves the formation of a crack of a critical size and its propagation with no further load increase, the dispersed failure mode requires many more dispersed fibre breaks prior to their coalescence. The qualitative transition with decreasing ρ , i.e., increasing s_F^2 was termed the brittle-to-tough transition by Curtin [17]. The probabilistic model of Harlow and Phoenix [8], and Smith [12] apply only to brittle bundles, and grossly overestimate failure probabilities in tough bundles. The validity of the weakest-global load sharing link according to Eq. (7) was shown by Ibnabdeljalil and Curtin [13] for $\rho \geq 2$. Curtin's [14] result on planar arrays was tested for $\rho \geq 3$ on bundles comprised of 2500 fibres or fewer.

The brittle-to-tough transition was observed in simulated bundle failures of Hedgepeth load sharing bundles by Mahesh et al. [6, 7]. They found that as ρ decreased below about a value of about 2, deviations from the weakest-link scaling given by Eq. (5) became more and more prominent, and the Hedgepeth bundle strength distribution tended toward that of the ELS bundle, Eq. (2). This was accompanied by a gradual suspension of the cluster growth type failure mode in favour of dispersed breaking. The bundles treated in the Monte-Carlo simulations of Mahesh et al. [6, 7] were comprised of fewer than $n = 1000$ fibres. It was therefore, not possible to ascertain if these conclusions would hold for very large n also.

Mahesh and Phoenix [11] found that simulations of one dimensional LLS bundles too show an apparent transition from the cluster growth mode to the dispersed mode, when ρ decreases, with the transition occurring close to $\rho = 1$. However, empirically obtained G_n^{LLS} distributions from simulations on bundle sizes as large as $n = 10^6$, clearly revealed that the weakest-link scaling, Eq. (5), remained valid for all ρ . This showed that bundle strength distribution remained in the brittle regime for all ρ . Although Mahesh and Phoenix [11] obtained

rigorous bounds on $W(\ell)$ valid for all ρ using the Chen-Stein theorem, they could not obtain a simple probabilistic model for $W(\ell)$.

It is not presently known if weakest-link scaling, Eq. (5), also applies to the two-dimensional LLS bundles. In two-dimensional bundles, fibres are distributed over a plane. Qualitatively, the stress concentration on intact neighbours of a cluster of breaks in two-dimensions is smaller than that in one-dimension, simply because the number of neighbours is larger in two dimensions. This may promote deviations away from the cluster growth mode, toward the ELS like dispersed fibre breaking mode, and lead to break down of the weakest-link scaling of the LLS bundle strength distribution. Also, if Eq. (5) holds in the two-dimensional case, the sequence of failure events that determine the weakest-link are presently unknown.

I.2. Overview of the present work

The present objective is to obtain conservative bounds for the strength distributions of composite bundles. Of the various load sharing models proposed in the literature [4, 5, 7, 13, 14, 18–20], the local load sharing (LLS) model imposes the severest overloads on the neighbours of broken fibres. This implies [12] that $G_n^{\text{LLS}}(\ell)$ conservatively bounds the strength distribution obtained assuming any of the more realistic load sharing models. Also, the usual modelling assumption that fibres are centred at the points of a regular lattice [4, 5, 7, 10, 12–14, 18–20] while being a good approximation, does not yield a strictly conservative bound [21] on the stress concentrations or strength distribution of realistic composites. To obtain a conservative bound, the fibre centres are assumed to be distributed following a Poisson point process in the present work.

Using Monte-Carlo simulations (Sec. II) of two-dimensional LLS bundles comprised of fibres distributed according to a Poisson point process of intensity γ over a unit square, it is presently shown that the bundle strength distribution obeys Eq. (5), but not Eq. (7). This result strongly suggests the absence of a brittle-to-tough transition in the two-dimensional case, just as in the one-dimensional case [11]. Furthermore, a probabilistic model for $W(\sigma)$ is presently constructed in Sec. III, which is valid for all ρ . This model visualises the LLS bundle as a collection of smaller ELS bundles, and models the weakest link event as the successive failure of neighbouring ELS bundles under overloads produced by the failure. The model thus envisages an additional size scale between that of the fibre and the LLS bundle, viz. that of the intermediate ELS bundle. At large ρ , the ELS bundle includes only a single fibre, so that the model coincides with that of Smith et al. [10]. However, with decreasing ρ , the ELS bundles encompass increasingly greater number of fibres, and the model predictions deviate from Smith et al. [10] significantly. The present model does not coincide with that of Curtin [14], for any ρ . These

deviations provide insights into the failure modes of LLS bundles. The weakest-link distributions obtained empirically from Monte-Carlo simulations and those predicted by the probabilistic model are compared in Sec. IV, and excellent agreement is shown.

II. FAILURE SIMULATIONS

Monte-Carlo simulations are performed in order to determine the empirical strength distribution of LLS bundles. In each simulation, fibres are distributed according to a Poisson process of intensity γ in a unit square in the plane, $[0, 1] \times [0, 1] \subset \mathbb{R}^2$, and assigned Weibull distributed strengths with exponent ρ , following Eq. (8). Three bundle sizes, $\gamma = 10^3, 10^4$ and 10^5 and many Weibull exponents ρ in the range from 0.1 to ∞ are investigated. For each combination of ρ and γ , $n_{\text{sim}} = 500$ simulations are performed, each with a different realisation of fibre positions and strengths.

Probabilistic models of composite failure assume that fibres of non-zero circular cross-sectional area are centred at the points of a regular lattice [6, 7, 10, 13, 14]. This case corresponds to zero fibre density fluctuations. More realistically, fibres would be distributed such that their centres follow the statistics of hard non-interpenetrating disks. This statistics of this distribution depends on the fibre volume fraction [22]. The assumption of fibres centred at the points of a regular lattice, while being a good approximation at high fibre volume fractions, does not yield a conservative bound on strength of the realistic bundle.

The point density fluctuations in the presently considered Poisson process can be no less than that in the case of hard non-interpenetrating disks [22, p. 147]. Higher point density fluctuations implies larger stress concentrations on intact neighbours of broken fibres, which in turn, implies a more localised brittle failure mode, and smaller bundle strength [12, 21]. Therefore, the bundle strength predicted using the present Poisson point distributed will be more conservative than in the case of random distributions of hard non-interpenetrating discs, for any fibre volume fraction.

Barring the implementation of load transfer from broken to intact fibres, the procedure adopted in these simulations is the same as that given by Mahesh et al. [6, 7, 11]. Briefly, the simulation is divided into as many steps as the number of fibres in the simulation cell (central domain). Since the simulation cell has unit area, the applied stress per fibre equals the applied load per fibre. The applied stress per fibre, $\sigma(= \ell)$ is incremented or decremented at every step to fail exactly one additional fibre. Following this, the stress concentration on all surviving fibres is updated using the load sharing rule, and the process is repeated until all the fibres in the simulation cell are broken. The maximum value attained by σ over all breaks is recorded as the bundle strength, $\bar{\sigma}_j$ for the j -th simulation. These are ordered $\bar{\sigma}_1 \leq \bar{\sigma}_2 \leq \dots \leq \bar{\sigma}_{n_{\text{sim}}}$ and mapped to empirical proba-

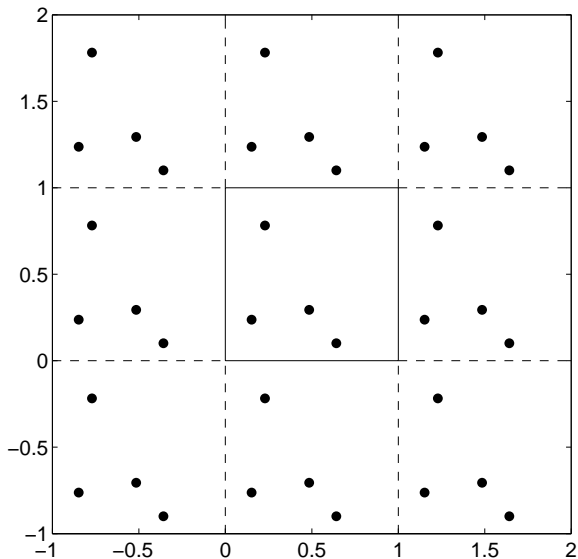


FIG. 1: (Colour online) A periodic central domain with $\gamma = 4$ is obtained by surrounding the cell with 8 identical cells.

bility levels $G_\gamma(\bar{\sigma}_j) = j/(n_{\text{sim}} + 1)$, $j = 1, 2, \dots, n_{\text{sim}}$ in order to obtain the empirical bundle strength distribution function.

Fibres abutting the edges of unit square simulation domain are surrounded on average by fewer fibres, which distorts the load sharing rule for such boundary fibres. To avoid this distortion, periodic boundary conditions are imposed on the unit square simulation domain by surrounding the unit square domain by eight identical domains, wherein the fibres are distributed exactly as in the central domain, as shown in Fig. 1. Fibres in the neighbouring domains are not assigned strengths; they are linked to their image in the central domain, and are assumed to fail when their image in the central domain fails.

The local load sharing (LLS) rule implemented presently is now discussed. Consider a bundle of n fibres, of which r fibres are broken already. Let the surviving $n - r$ fibres be located at (x_i, y_i) , $i = 1, 2, \dots, n - r$. An example of such a bundle is shown in Fig. 2a. Each of the surviving fibres i is associated with a Voronoi cell [23]:

$$C_i^r = \{(x, y) : \|(x - x_i, y - y_i)\| \leq \|(x - x_j, y - y_j)\|, \forall j \neq i\}, \quad (10)$$

$i, j \in \{1, 2, \dots, n - r\}$. In Eq. (10), $\|\cdot\|$ is defined as:

$$\|(a, b)\| = \min \left\{ \sqrt{a^2 + b^2}, \sqrt{(1 - a)^2 + b^2}, \sqrt{a^2 + (1 - b)^2}, \sqrt{(1 - a)^2 + (1 - b)^2} \right\} \quad (11)$$

$\forall 0 \leq a, b \leq 1$ to reflect periodicity in the x and y directions. Let A_i^r denote the area of Voronoi cell C_i^r .

Let σ_j^r denote the stress per fibre imposed upon the bundle with r broken, and $n - r$ intact fibres in the j -th weakest simulation specimen. The load applied to fibre i

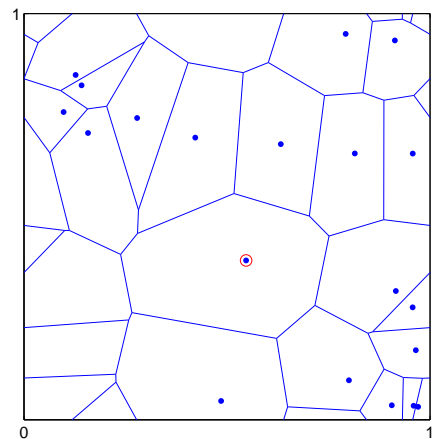
is then $\sigma_j^r A_i$. Let the Weibull distributed fibre strength of i be L_i . Then, the index i^* of the next fibre to break is

$$i^* = \operatorname{argmin}_{i=1, \dots, n-r} (L_i/A_i), \quad (12)$$

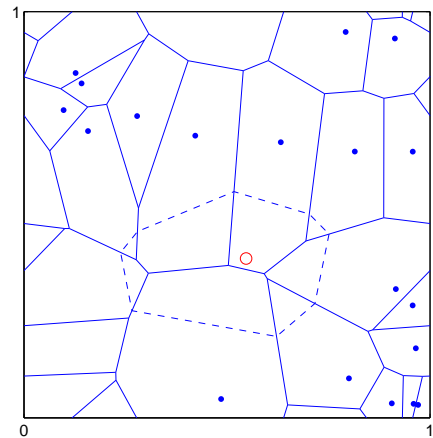
and the applied stress at which the next fibre will break is

$$\sigma_j^{r+1} = \min_{i=1, \dots, n-r} (L_i/A_i). \quad (13)$$

Let i^* be the fibre shown as an encircled point in Fig. 2a. Upon its failure, i^* and $C_{i^*}^r$ are deleted, and the area of cell $C_{i^*}^r$ is divided amongst its neighbours, as shown in Fig. 2b. This represents the most time consuming step; an efficient deletion algorithm has been given by Devillers [24].



(a)



(b)

FIG. 2: (Colour online) The periodic Voronoi tessellation of a unit square with $n = 20$ points (a) before, and (b) after the deletion of one point, shown encircled in (a).

Carrying this process forward for $r = 1, 2, \dots, n$ results in complete failure of the LLS bundle. The bundle strength is defined as

$$\bar{\sigma}_j = \max_{r=1, 2, \dots, n} \sigma_j^r, \quad j = 1, 2, \dots, n_{\text{sim}}. \quad (14)$$

The just described LLS rule involves no matrix operations, and is therefore, computationally the fastest load sharing model for two dimensional bundles. This allows the simulation of fibre bundles comprised of as many as 10^5 fibres. For comparison, the number of fibres in the largest elastic load sharing planar simulation cell of Curtin [14] was 2500. Assuming Hedgepeth load sharing, Mahesh et al. [7], included at most 900 fibres in their simulation cell. The empirical distributions obtained from the present simulation cells with a larger number of fibres extend deeper into the lower tail of the weakest-link distribution function. This allows a better check of the probability models.

A number of realistic load sharing models have been proposed in the literature [4, 5, 7, 13, 14, 20]. Let $G_n^{\text{real}}(\ell)$ denote the strength distribution of a bundle of n fibres obeying any of the realistic load sharing rules. Let $W^{\text{real}}(\ell) = 1 - (1 - G_n^{\text{real}}(\ell))^{1/n}$ be the associated n -independent weakest-link distribution. The LLS rule imposes more severe overloads on the neighbours of a fibre break, or a cluster of breaks, than any of the realistic load sharing models. This implies, according to the probability model of Smith [12], that $W^{\text{real}}(\ell) \leq W(\ell)$, or $G^{\text{real}}(\ell) \leq G^{\text{LLS}}(\ell)$. That is, the LLS rule conservatively bounds the strength distribution obtained from any of the realistic load sharing models.

III. PROBABILISTIC MODEL

The empirical strength distribution of LLS bundles, $G_\gamma(\bar{\sigma}_j)$, down to a probability level of $1/(n_{\text{sim}} + 1)$ can be obtained from n_{sim} Monte-Carlo simulations for fixed ρ and γ . It is typically computationally infeasible to perform more than a few hundred simulations. Strength distribution predictions in the high reliability regime, $G_\gamma(\bar{\sigma}_j) \leq 10^{-6}$ is therefore, normally inaccessible through Monte-Carlo simulations alone. This motivates the need for a probabilistic model that captures the distribution obtained from Monte-Carlo simulations, and which can readily be extended into the high reliability regime.

The present probabilistic model regards the LLS bundle as a collection of many ELS bundles, each of which in turn, may contain one or more fibres. The intermediate scale of the ELS bundles plays a key role in the model, especially at small ρ . The elementary failure event in the present model is the failure of an ELS bundle, unlike in Harlow and Phoenix's [8] or Smith et al.'s [10, 12] models, where the elementary failure event is the failure of an individual fibre.

III.1. Poisson-Voronoi tessellation

Let $\chi = \{(x_i, y_i) : i \geq 1\}$ denote a homogeneous Poisson point process [16] of intensity γ in \mathbb{R}^2 restricted to the unit square, $[0, 1] \times [0, 1] \subset \mathbb{R}^2$, which specifies the fibre locations. Let χ' denote the Poisson point sub-process

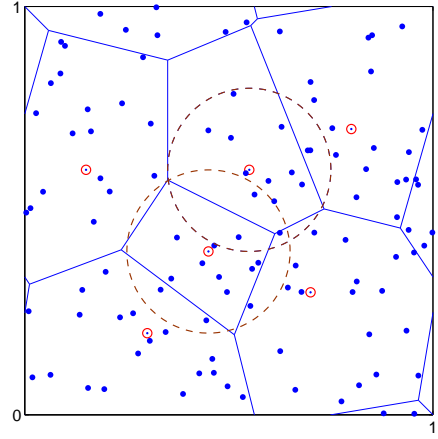


FIG. 3: (Colour online) Poisson process χ represented by the small blue dots, and the sub-process χ' represented by the encircled blue dots assuming $p = 1/10$. Each point in χ' is associated with an ELS bundle comprised of $m = 15$ points of χ .

derived by sampling from χ with probability $p \in [0, 1]$: $\chi' = \{(x_{i'}, y_{i'}) \in \chi : U_{i'} \leq p\}$, where $\{U_j \in [0, 1] : j \geq 1\}$ denotes a sequence of uniformly distributed independent random variables. The expected number of points in χ and χ' are then γ and $p\gamma$, respectively. Each point $(x_{i'}, y_{i'}) \in \chi'$ represents an equal load sharing (ELS) bundle comprised of $m \geq 1/p$ fibres.

An example of this scheme is presented in Fig. 3. In this example, the Poisson process χ of intensity $\gamma = 50$ is represented by the small blue dots, each of which locates a fibre. The sub-process χ' is shown by encircled blue dots assuming $p = 1/10$. Each point in χ' is associated with an ELS bundle comprised of $m = 15$ points of χ . Two such ELS bundles are shown as circles drawn using dashed lines. Note that neighbouring ELS bundles may overlap, i.e., share common points in χ . Fig. 3 also shows a Voronoi tessellation of the χ' process. It is important to notice that the tessellation is not of the χ process.

The neighbours of $(x_{i'}, y_{i'}) \in \chi'$, denoted $\mathcal{N}_{i'}$, are those points whose Voronoi cells share a common edge with $C_{i'}$. The number of neighbours of $(x_{i'}, y_{i'}) \in \chi'$ equals the number of sides of $C_{i'}$ and is denoted $N_{i'}$. The area of $C_{i'}$ is denoted $A_{i'}$.

III.2. Tight clusters and load concentration

The present probabilistic model follows that of Smith et al. [10], with the key difference that ELS bundle failures are assumed to be the elementary events leading up to LLS bundle failure. In the present probabilistic model, LLS bundle failure initiates with the failure of an ELS bundle located at $i'_1 \in \chi'$. The load dropped by $i'_1 \in \chi'$ is then distributed amongst its neighbours, $C_{j'_1}, j'_1 \in \mathcal{N}_{i'_1}$, following local load sharing. Next one of the ELS bundles, say $i'_2 \in \mathcal{N}_{i'_1}$ is assumed to fail. The third step

involves the failure of one of the ELS bundles representing an intact neighbour of $\mathcal{N}_{i'_1}$ or $\mathcal{N}_{i'_2}$. Proceeding thus, a connected cluster of k failed ELS elements, i'_1, i'_2, \dots, i'_k is arrived at. It is additionally required that the connected cluster maintain an approximately circular shape at every stage of the failure process. Such a circular cluster of ELS bundle failures is called a ‘tight’ cluster of breaks, following the nomenclature of Mahesh et al. [7].

Derivation of approximate formulae to describe the stress state around a tight cluster of breaks is facilitated by observing the following connection between the Poisson process and a regular hexagonal lattice. The discrete density of the number of neighbours of a typical point in a Poisson-Voronoi tessellation, $\Pr\{N_i = l\}$, $l = 3, 4, \dots$, due to Calka [25] has mode $l_{\text{mode}} = 6$. The number of neighbours of a fibre in Smith et al.’s. [10] hexagonal lattice is also 6. This similarity is presently exploited to approximate the number of neighbours of a tight cluster of k failed elements.

In Smith et al.’s [10, Fig. 2 (d)] hexagonal lattice, the number of lattice points in a tight cluster of r ‘rings’ is $k = 1 + 6 + \dots + 6(r - 1) = 3r(r - 1) + 1$. The number of neighbours whose failure will preserve the circular ‘tight’ shape of the cluster is $6(r - 1)$. Eliminating r , the number of critical neighbouring points surrounding a tight cluster of k breaks, is approximately

$$n_k = 2\sqrt{3k} - 3, \quad k = 1, 2, \dots \quad (15)$$

The overload on each of these n_k neighbouring elements is k/n_k , approximately. To account for the error of approximation, a fitting parameter M is introduced. The actual overload is taken to be Mk/n_k , where M is understood to be of the order of 1. Thus, the load concentration factor on the n_k neighbouring elements is

$$K_k = 1 + Mk/n_k. \quad (16)$$

In Calka’s [25] discrete distribution noted above, $\Pr\{N_i < 6\} \approx 0.38$, while $\Pr\{N_i > 6\} \approx 0.33$. The discrete density function is thus weighted toward the former, i.e., n_k given by Eq. (15) is more likely to be an over-count than an undercount of the number of neighbours at least for $k = 1$. Also, the most overloaded neighbouring point will be subjected to more than the average stress concentration of k/n_k . For both these reasons, it is expected that $M > 1$ in Eq. (16).

III.3. Weakest-link event

Let σ be the uniform far-field tensile stress per fibre imposed on the bundle χ . Because the bundle cross-sectional area is unity, σ is also the load per fibre imposed. The expected total tensile load imposed on the bundle is then $\sigma\gamma$. Each point $(x_i, y_i) \in \chi'$ is associated with an equal load sharing (ELS) bundle comprised of $m \geq 1/p$ fibres drawn from χ . Let $E_m(\sigma)$ denote its strength distribution. Expressions for $E_m(\sigma)$ are presented later in Sec. III.4.

Following Smith et al. [10], the weakest-link event underlying LLS bundle failure is assumed to begin with the failure of the weakest of the approximately $p\gamma$ ELS bundles. The overload K_1 produced on the n_1 neighbours of the weakest bundle following Eqs. (15) and (16) is then assumed to fail one of them. This process of failure and overloading is continued up to the failure of k ELS bundles. According to this model, probability of failure of the LLS bundle obeys weakest-link scaling, and is approximately given by

$$G_\gamma(\sigma) = \lim_{k \rightarrow \infty} 1 - (1 - W_k(\sigma))^{p\gamma}, \quad (17)$$

where,

$$W_k(\sigma) = E_m(\sigma) \{1 - (1 - E_m(K_1\sigma))^{n_1}\} \times \\ \{1 - (1 - E_m(K_2\sigma))^{n_2}\} \times \\ \dots \{1 - (1 - E_m(K_k\sigma))^{n_k}\}. \quad (18)$$

According to Eq. 17, $p = 1$ signifies the association of the weakest-link failure event with every fibre, while $p < 1$ signifies the same for every $(1/p)$ -th fibre, on average. The requirement that $m \geq 1/p$ stated above ensures that every fibre is part of at least one ELS bundle.

III.4. ELS bundle strength distribution

Consider an ELS bundle of m fibres, each of which fails following the distribution function $\hat{F}(\sigma)$ under imposed remote stress σ . As noted in Sec. I, $E_m(\sigma)$ will be Gaussian with mean and standard deviation given by Eqs. (3) and (4), respectively, provided $m \rightarrow \infty$. For small m , however, $E_m(\sigma)$ is given by an efficient and accurate recurrence relation due to McCartney and Smith [26]:

$$E_m(\sigma) = \hat{F}^m(\sigma) - \sum_{r=0}^{m-1} \binom{m}{r} \phi_r \left\{ \hat{F}(\sigma) - \hat{F}\left(\frac{\sigma}{m-r}\right) \right\}^{m-r}, \quad (19)$$

where, $\phi_0 = 1$, and

$$\phi_r = \hat{F}^m\left(\frac{\sigma}{m-r-1}\right) - \\ \sum_{p=0}^{r-1} \binom{r}{p} \phi_p \left\{ \hat{F}\left(\frac{\sigma}{m-r-1}\right) - \hat{F}\left(\frac{\sigma}{m-r}\right) \right\}^{r-p}. \quad (20)$$

III.5. Fibre failure probability

It only remains to determine the strength distribution of fibres making up the ELS bundles as a function of the applied stress per fibre, σ . Let the fibre strengths be Weibull distributed with exponent ρ , according to Eq. (8). In that equation, the fibre strength L refers to the maximum load it can carry. The load, in turn, is the product of the applied stress per fibre, σ and the area of the its Voronoi cell, A . The distribution of A

in a Poisson-Voronoi tessellation is yet an unsolved problem of stochastic geometry. Empirical distributions for A can, however, be obtained through simulations. Following the simulation approach, a number of authors have found that the gamma distribution captures the area distribution obtained from simulations quite well. Here, the following expression, given by Kiang [27]

$$\Pr\{A \leq a\} = \frac{c}{\Gamma(c)} \int_{\alpha=0}^a (c\alpha)^{c-1} \exp(-c\alpha) d\alpha, \quad (21)$$

is taken to describe the area distribution of Voronoi cells in a Poisson-Voronoi tessellation, with $c = 4$ for point distributions in \mathbb{R}^2 . In

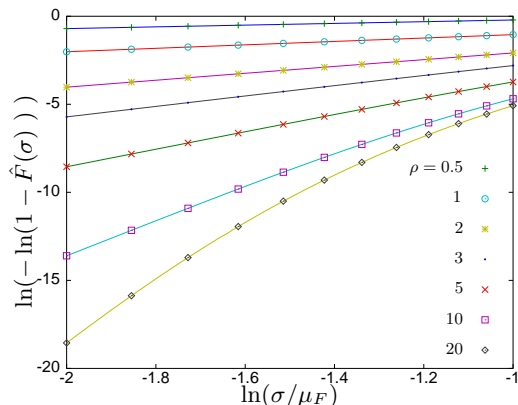


FIG. 4: (Colour online) Fibre strength distribution as a function of the applied stress per fibre, for a range of ρ given by Eq. (22).

If L_i denotes the strength of fibre i , and A_i the area of its Voronoi cell, the fibre failure event corresponds to $[L_i \leq \sigma A_i]$. It is physically reasonable to assume that L_i and A_i are independent. Therefore, the probability of failure of fibre i is given as

$$\begin{aligned} \hat{F}(\sigma) &= \Pr\{L_i \leq \sigma A_i\} \\ &= \frac{c}{\Gamma(c)} \int_{a=0}^A (ca)^{c-1} \exp(-ca) F(\sigma a) da, \quad (22) \\ &= 1 - \frac{c^c}{\Gamma(c)} \int_{a=0}^{\infty} a^{c-1} \exp(-(ca + (\sigma a)^\rho)) da. \end{aligned}$$

The form of $F(\sigma a)$ in the second step above follows from Eq. (8). The fibre strength distributions for a range of ρ given by Eq. (22) is shown in Fig. 4.

IV. RESULTS

Failure patterns and strength distributions obtained from the Monte-Carlo simulations described in Sec. II are now presented, and compared with predictions of the probabilistic model of Sec. III.

As stated in Sec. II, empirical strength distributions $G_\gamma(\bar{\sigma}_j)$, for $j = 1, 2, \dots, n_{\text{sim}}$ are obtained from $n_{\text{sim}} =$

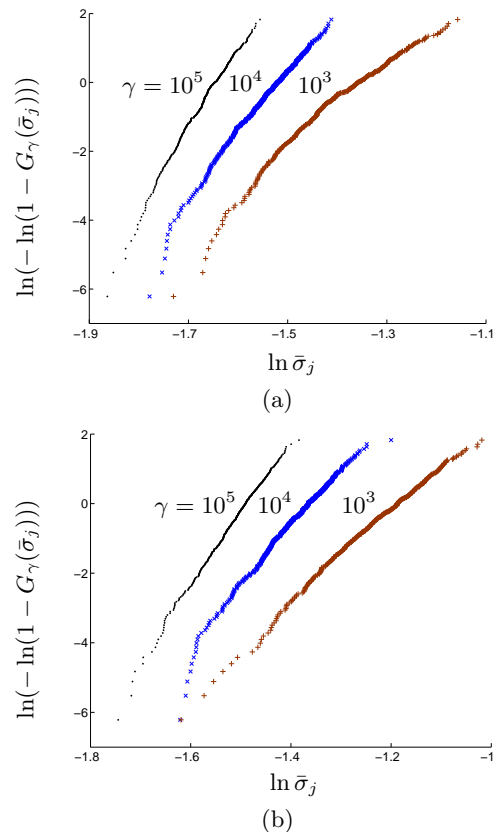


FIG. 5: (Colour online) Empirical LLS bundle strength distributions, $G_\gamma(\bar{\sigma})$ obtained from Monte-Carlo simulations for $n_{\text{sim}} = 500$ random realisations of (a) $\rho = 1$, and (b) $\rho = 10$ LLS bundles, plotted on Weibull probability paper.

500 realisations of LLS bundles for a range of Poisson intensities γ and Weibull exponent ρ . Fig. 5 shows the obtained empirical distributions plotted on Weibull probability paper for $\gamma = 10^3, 10^4$ and 10^5 and Weibull exponents $\rho = 1$ and $\rho = 10$. In these coordinates, Weibull distributions plot as straight lines. Since the obtained empirical distributions are curved downward, it follows that $G_\gamma(\bar{\sigma}_j)$ is not Weibull distributed, even though the individual fibre strengths are. It is also clear that bundles with larger γ are weaker: for any fixed probability level G_γ , the larger bundles has a smaller strength, $\bar{\sigma}_j$.

If the strength statistics of the LLS bundle with the random fibre strengths and spacing were similar to that of an ELS bundle, bundle strengths would be Gaussian distributed, following Eq. (2). To check this possibility, Fig. 6 plots the same empirical distributions shown in the previous Fig. 5, on Gaussian probability paper. In these coordinates, normal distributions plot as straight lines. It is clear from Fig. 6a and Fig. 6b corresponding to $\rho = 1$ and $\rho = 10$, respectively, that LLS bundle strengths do not plot as straight lines. They have an upward curvature, which indicates that LLS bundle strengths are not Gaussian distributed.

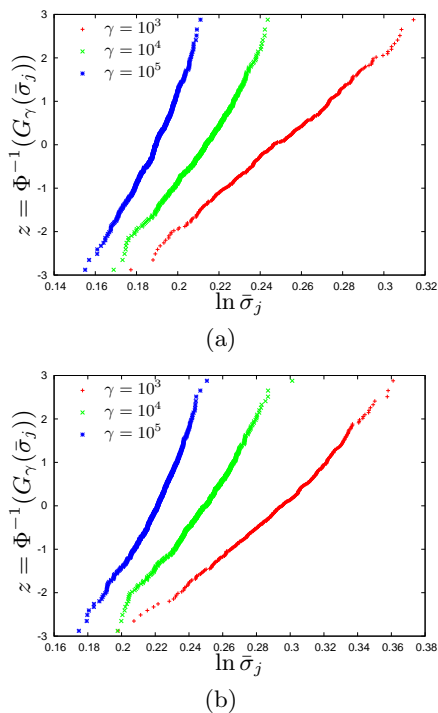


FIG. 6: (Colour online) Empirical LLS bundle strength distributions, $G_\gamma(\bar{\sigma})$ obtained from Monte-Carlo simulations for $n_{\text{sim}} = 500$ random realisations of (a) $\rho = 1$, and (b) $\rho = 10$ LLS bundles, plotted on Gaussian probability paper.

IV.1. Critical bundle

Each step of the Monte-Carlo simulation entails incrementing or decrementing the applied stress per fibre, σ_j^r so as to augment the number of breaks by 1 (Sec. II). The history of σ_j^r versus the number of breaks, r in the median (250th weakest out of $n_{\text{sim}} = 500$ simulations) $\gamma = 10^3$, and $\rho = 1$ simulation is shown in Fig. 7a. Although both increments and decrements of σ_j^r are plotted, only σ_j^r increments are physically meaningful, because in a practical experiment, the applied stress will be monotonically increased. Accordingly, the ‘physical’ σ_j^r curve, obtained by taking the cumulative maximum value (upper envelope) derived from the σ_j^r curve is also shown in Fig. 7a. The σ_{250}^r - r plot shown in Fig. 7a peaks at the bundle strength $\bar{\sigma}_{250} = 0.246$, at which point the number of broken fibres is 362. The distribution of intact (dots) and broken (circles) fibres at $r = 362$ breaks is shown in Fig. 7b. It appears that the broken fibres are widely dispersed all over the bundle domain. No large tight cluster (Sec. III.2) is discernible.

A very different response is observed in Fig. 8 corresponding to the median $\gamma = 10^3$, and $\rho = 10$ bundle. The peak of the σ_j^r versus the number of breaks, r curve is reached after the formation of only 13 breaks under applied stress per fiber $\bar{\sigma}_{250} = 0.321$ in Fig. 8a. Furthermore, as is clear from Fig. 8b, these breaks are tightly clustered together into two groups.

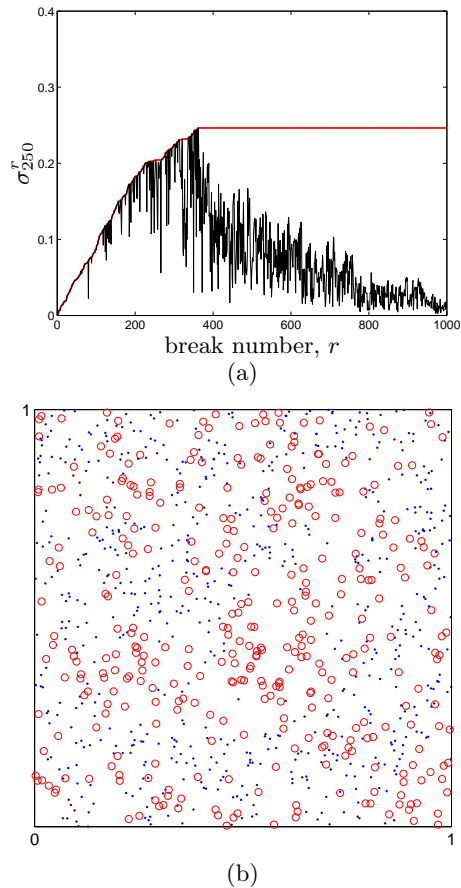


FIG. 7: (Colour online) (a) The fluctuating curve shows the evolution of applied stress per fibre σ_{250}^r with the number of fibre breaks, r in the median $\rho = 1$, $\gamma = 10^3$ simulated LLS bundle. The flat portion of the red curve marks represents the bundle strength $\bar{\sigma}_{250}$. (b) Configuration of broken and intact fibres at the point of formation of the critical cluster. σ_j^r and $\bar{\sigma}_r$ are defined in Sec. II.

Qualitative understanding of this difference can be obtained by recognising that the standard deviation of the Weibull distribution, Eq. (9), corresponding to $\rho = 1$ is 1, while that corresponding to $\rho = 10$ is about 0.11. The higher ρ thus has much less spread of the fibre strengths. In this circumstance, the stress overload due to the failure of a neighbouring fibre will significantly enhance the probability of failure of a fibre. Successive fibre failures will be controlled by stress concentrations, which will therefore be clustered. In the $\rho = 1$ median specimen on the other hand, because of the wide scatter in fibre strengths overloads due to the failure of neighbouring fibre will not significantly enhance fibre failure probability. The sequence of fibre failures will be controlled by the ordering of fibre strengths, and the weakest fibres can be expected to be distributed uniformly all over the bundle, as in Fig. 7b.

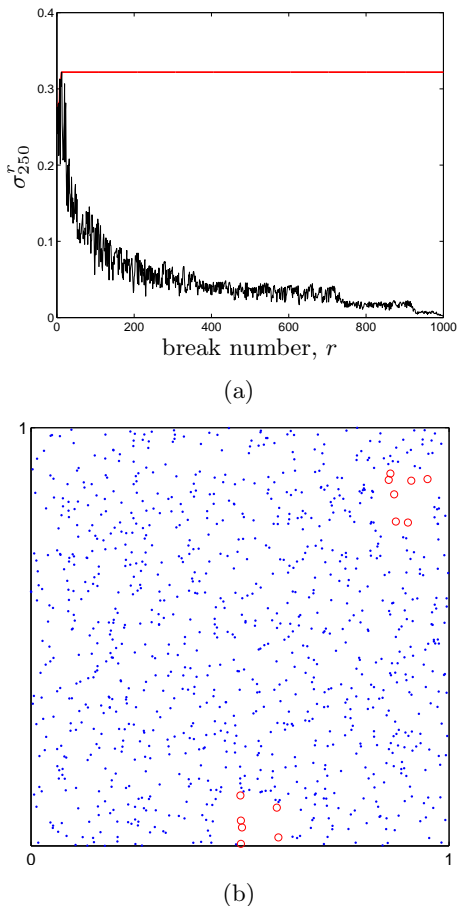


FIG. 8: (Colour online) (a) The fluctuating curve shows the evolution of applied stress per fibre σ_{250}^r with the number of fibre breaks, r in the median $\rho = 10$, $\gamma = 10^3$ simulated LLS bundle. The flat portion of the red curve represents the bundle strength $\bar{\sigma}_{250}$. (b) Configuration of broken and intact fibres at the point of formation of the critical cluster. σ_j^r and $\bar{\sigma}_r$ are defined in Sec. II.

IV.2. Weakest-link distribution

The weakest-link distribution is defined as

$$W_\gamma(\bar{\sigma}_j) = 1 - (1 - G_\gamma(\bar{\sigma}_j))^{1/\gamma}, \quad (23)$$

by replacing n in Eq. (5) by γ . $W_\gamma(\bar{\sigma}_j)$ corresponding to the three decades of γ values studied are plotted in Fig. 9 for four values of $\rho \geq 0.5$. The abscissae have been normalized by the mean strength, given by Eq. (9). It is patently clear from Fig. 9 that $W_\gamma(\bar{\sigma}_j)$ is independent of γ for a fixed ρ : W_{10^3} , W_{10^4} and W_{10^5} collapse onto a single master curve, for all $\rho \geq 0.5$. This justifies dropping the subscript γ and denoting the weakest-link distribution by $W(\bar{\sigma}_j)$. Although for clarity only four values of ρ are shown in Fig. 9, the foregoing observation is found to be true for all simulated values of $\rho \geq 0.5$.

For $\rho < 0.5$, collapse of the empirically obtained weakest-link distributions does not occur. Fig. 10 shows that at $\rho = 0.2$, whereas the simulated weakest-link distribution for $\gamma = 10^4$ and 10^5 collapse into a single curve,

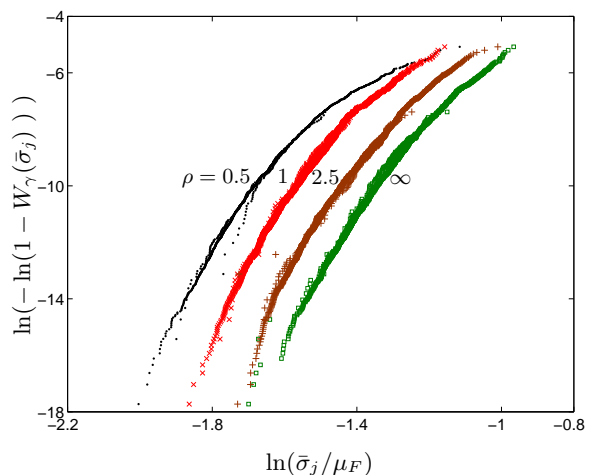


FIG. 9: (Colour online) Weakest-link distributions, defined in Eq. (23), derived from the empirical strength distributions corresponding to $\gamma = 10^3, 10^4$, and 10^5 , for $\rho \geq 0.5$. $W_\gamma(\bar{\sigma}_j)$ is found independent of γ .

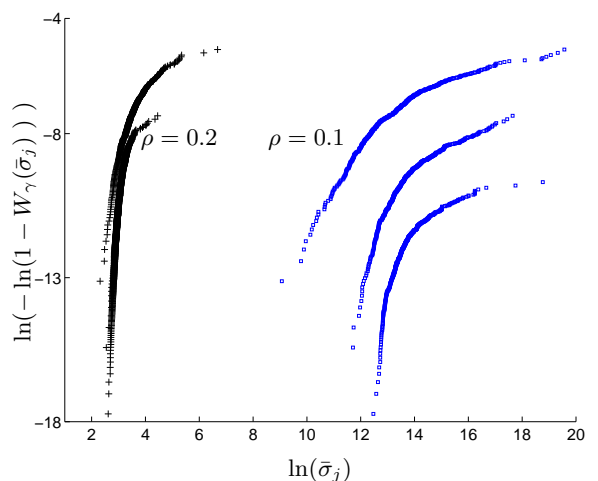


FIG. 10: (Colour online) Weakest-link distributions of $\rho = 0.2$ and $\rho = 0.1$ bundles with $\gamma = 10^3, 10^4$ and 10^5 .

that for $\gamma = 10^3$ does not. At $\rho = 0.1$, none of the three curves coincide with any other.

IV.3. Weakest ELS-bundle distribution

It is now attempted to verify the weakest ELS-bundle scaling given by Ibnabdeljalil and Curtin [13] and Curtin [14], given previously in Eqs. (6) and (7). Figs. 11a and 11b show the weakest ELS link distribution, W^{n_c} corresponding to $n_c = 200$ for $\rho = 1$ and to $n_c = 20$ for $\rho = 200$, respectively, on Gaussian probability paper. The collapse of the curves corresponding to $\gamma = 10^3, 10^4$ and 10^5 onto a single curve for both values of ρ implies that $W^{n_c}(\bar{\sigma}_j)$ is indeed independent of γ . This is not surprising in light of the collapse observed in

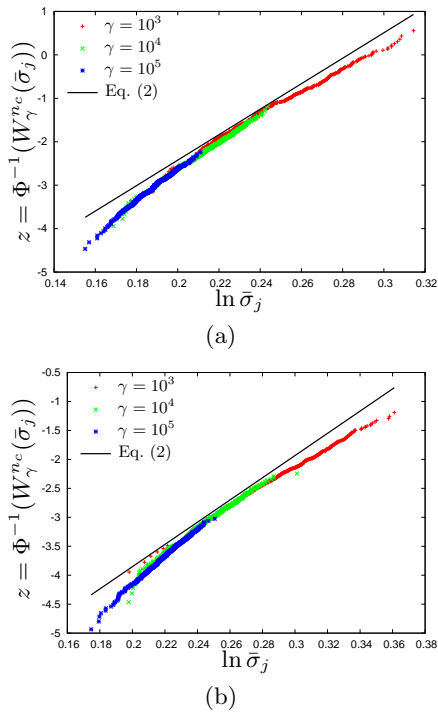


FIG. 11: (Colour online) Weakest ELS-bundle distributions, defined in Eq. (6), derived from the empirical strength distributions corresponding to $\gamma = 10^3$, 10^4 , and 10^5 , for (a) $\rho = 1$ with $n_c = 200$ and (b) $\rho = 10$ with $n_c = 20$.

Fig. 9 onto a single master curve. The collapsed master curves are however, not straight lines. This indicates that they are not Gaussian distributed. The straight lines in Figs. 11a and 11b correspond to the strength distribution of an n_c fibre ELS bundle, given by Eq. (2), shifted vertically upward by 2.5 and 6.1 for $\rho = 1$ and $\rho = 10$, respectively. These shifts amount to adjusting the mean strength of the ELS bundle. They were also needed in the work of Curtin [14], as noted below Eq. (7).

The values of n_c corresponding to $\rho = 1$ and $\rho = 10$ in Fig. 11 are chosen to best bring the slope of Daniels' Gaussian distribution into agreement with that of the empirical distribution. The slope corresponds to the standard deviation in Gaussian probability paper. Increasing the value of n_c beyond the present values tends to straighten out the empirical distributions, i.e., makes them more Gaussian, but, destroys the near agreement between the weakest ELS-bundle distribution and that given by Eq. (2). On the other hand, decreasing the value of n_c below the present values increases the curvature of the collapsed master curve, i.e., makes it even more non-Gaussian. These observations show that the scaling given by Eqs. (6) and (7) does not apply to the present LLS bundle strength.

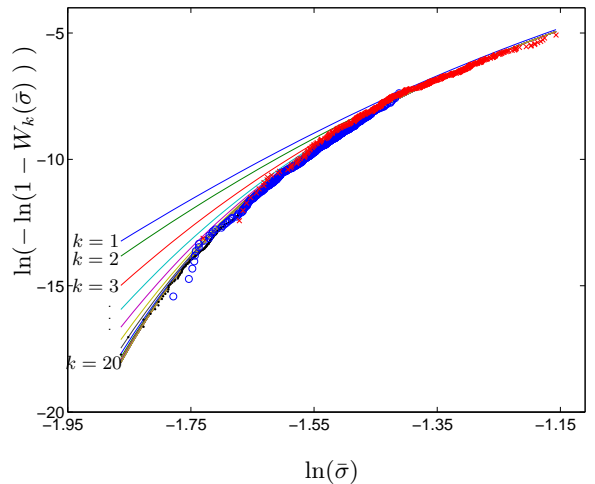


FIG. 12: (Colour online) The model predicted weakest-link probability $W_k(\bar{\sigma})$ (Eq. (18)) of obtaining a failed tight k -cluster in $\rho = 1$ LLS bundles.

IV.4. k -failure event

In the present probabilistic model, LLS bundle strength is represented as a continuous variable, $\bar{\sigma}$, without subscripts that identify the simulation number. Fig. 12 shows the weakest-link probability, $W_k(\bar{\sigma})$, of obtaining a failed tight k -cluster for $k = 1, 2, \dots, 20$ for $\rho = 1$ LLS bundles. This probability is predicted using Eq. (18) and taking ELS bundle size, $m = 25$, $p = 1/3$, and $M = 1.65$. It is seen that the model predictions accurately capture the empirically obtained weakest-link distribution, previously also shown in Fig. 9.

Convergence of the $W_k(\bar{\sigma})$ with increasing k happens for smaller k at higher $\bar{\sigma}$. At the highest $\bar{\sigma}$, convergence occurs already at $k = 1$. Even at the lowest value of $\bar{\sigma}$, convergence is practically complete by about $k = 10$. Denoting

$$W(\bar{\sigma}) = \lim_{k \rightarrow \infty} W_k(\bar{\sigma}), \quad (24)$$

it is clear that the rate of convergence is quite rapid.

For any given $\bar{\sigma}$, the value of k for which convergence is practically complete can be taken to indicate the size of the critical cluster. For the median $\rho = 1$ specimen of Fig. 7, the $\ln(\bar{\sigma}) = \ln(0.246)$ corresponds in Fig. 12 to $k = 2$. Multiplying by the number of fibres per bundle, $m = 25$, the weakest-link event in this bundle is triggered by the failure of a tight cluster of about 50 fibres. However, the identity of these 50 fibres is difficult to establish from Fig. 7b, given the seemingly dispersed breaking observed.

In the present $\rho = 10$ LLS bundles too, $W_{10}(\bar{\sigma})$ fits the empirically obtained weakest-link distribution very well. This suggests that the rate of convergence of the model is insensitive to ρ . The weakest-link probability, $W_k(\bar{\sigma})$, for $\rho = 10$ LLS bundles is similarly shown in Fig. 13. The assumed model parameters are ELS bundle size, $m = 1$, $M = 2.7$ and $p = 1$. Here, the load level

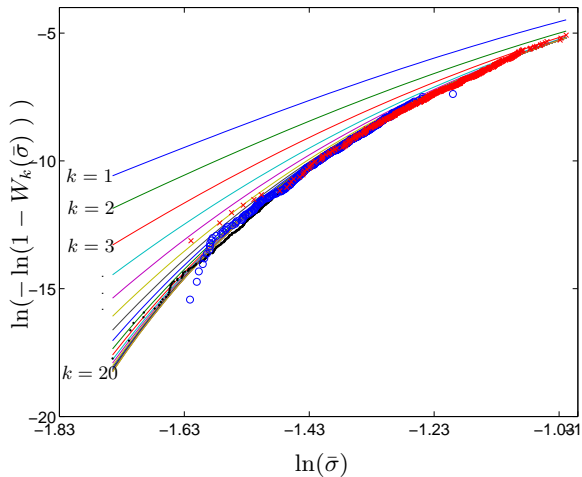


FIG. 13: (Colour online) The model predicted weakest-link probability $W_k(\bar{\sigma})$ (Eq. (18)) of obtaining a failed tight k -cluster in $\rho = 10$ LLS bundles.

of the median specimen, $\ln(\bar{\sigma}) = \ln(0.321)$ corresponds to $k = 4$ or $k = 5$. The critical cluster in this case, may have been a subset of either of the two groups of broken fibres shown in Fig. 8b.

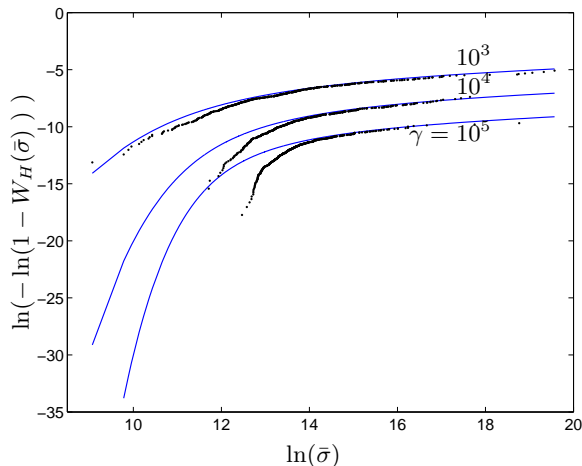


FIG. 14: (Colour online) Comparison of the empirical distributions with Eq. (26) for $\rho = 0.1$ for $\gamma = 10^3$, 10^4 and 10^5 bundles.

Attention is now turned to the regime $\rho < 0.5$. This regime is characterised by extremely large fibre strength variance. Corresponding to $\rho = 0.1$, Eq. (9) gives $\mu_F \approx 4 \times 10^6$ and $s_F^2 \approx 2 \times 10^{18}$. This indicates that a typical bundle will contain very strong fibres with high probability. Suppose bundle failure coincides with the failure of the strongest fibre therein. The probability of that all the fibres in a γ -bundle will fail under load $\bar{\sigma}\gamma$, applied per fibre is

$$H(\bar{\sigma}) = F^\gamma(\bar{\sigma}\gamma), \quad (25)$$

and the weakest-link calculated from this distribution would be

$$W_H(\bar{\sigma}) = 1 - (1 - H(\bar{\sigma}))^{1/\gamma}. \quad (26)$$

Fig. 14 compares the bundle strength distribution obtained from simulations of $\gamma = 10^3$, 10^4 and 10^5 bundles with $\rho = 0.1$, with the weakest-link distribution given by Eqs. (25) and (26). The evidently good comparison in the upper tail of the distribution validates the hypothesis that at small ρ , bundle failure in the present simulations coincides with the failure of the strongest fibre.

The agreement shown in Fig. 14, and the hypothesis underlying it, cannot persist indefinitely as γ is increased with ρ fixed. For a sufficiently large γ , which is likely to be much larger than 10^5 , the strongest fibre will not be strong enough to carry the entire bundle load, and the dominant failure mode must revert to that given in Sec. III. Monte-Carlo failure simulations of such gigantic bundles appear to be well out of reach with the present computational resources.

Hitherto, a distinction has been made between the regimes $\rho \geq 0.5$ and $\rho < 0.5$ in discussing bundle strength distributions. The foregoing considerations suggest that this distinction arises on account of computational limitations and not because the bundle failure mechanism itself undergoes a transition across $\rho = 0.5$. Therefore, hereafter, only the regime $\rho \geq 0.5$ will be discussed with the understanding that the physical mechanisms of bundle failure will continue to apply for all $\rho > 0$, for sufficiently large bundle size γ .

IV.5. Comparison of simulated and model distributions

TABLE I: Parameters used in the probabilistic model.

ρ	m	M	p
Eq. (8)	Sec. III.3	Eq. (16)	Sec. III.3
0.5	55	1.3	$\frac{1}{20}$
1	25	1.65	$\frac{1}{3}$
2	10	1.85	1
3	5	1.9	1
5	2	1.95	1
10	1	2.25	1
20	1	2.7	1
∞	1	2.9	1

Using the parameters listed in Tab. I, $W(\bar{\sigma})$ are determined using Eq. (24). It is seen from Tab. I that a monotonic variation of model parameters occurs with ρ : m increases, while M and p decrease with decreasing ρ . Representative comparisons of $W(\bar{\sigma})$ with the empirical weakest-link distributions obtained from simulations are shown in Fig. 15. The probabilistic model's predicted distribution and the empirically obtained distribution are seen to be in excellent agreement.

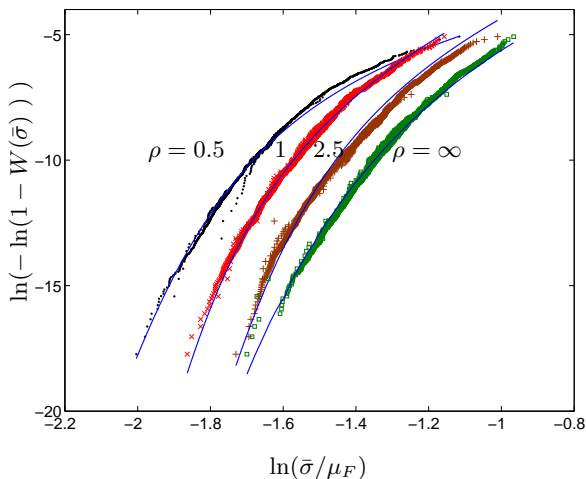


FIG. 15: (Colour online) Comparison of the empirical strength distribution obtained from Monte-Carlo simulations with the predictions of the probabilistic model, assuming the parameters listed in the Tab. I.

V. DISCUSSION

V.1. Summary

When fibre strengths have small variance, the failure of a single fibre typically overloads its neighbours to breakage also. Bundle failure proceeds by cluster growth like failure mode, and endows the bundle strength distribution with weakest-link scaling. Such bundles are termed brittle. For larger variance of fibre strength, the neighbour of a broken fibre is likely to possess sufficient strength to withstand the overload. Thus, with increasing fibre strength variance, fibre failures in an LLS bundle may not cluster together. That is, they may occur widely dispersed over the bundle domain. But, lack of proximity between successive fibre breaks characterises ELS bundle failure. This argument suggests [6] that as the fibre strength variance increases, LLS bundle strength must approach the ELS bundle strength.

The present results show that the above suggestion is not true for a planar LLS bundle. The correct qualitative argument for this case goes as follows: In an LLS bundle with large fibre strength variance, fibre breakages occur in a dispersed manner in the initial stages of bundle failure, as the overloads produced by single fibre failures are inadequate to fail their neighbours with high probability. However, there comes a point during dispersed fibre breakage when a cluster of breaks larger than a critical size, m , forms somewhere in the bundle at random. This cluster forms simply due to the fortuitous occurrence of weak fibres near each other. Beyond the point of formation of the m -cluster, dispersed fibre failure gives way to a clustered failure mode of m -sized bundles. The latter mode expands the original m -sized cluster. The requisite critical size m increases with increasing fibre strength variability. This failure mode endows the planar LLS

bundle strength distribution with weakest-link scaling.

V.2. Comparison with previous models

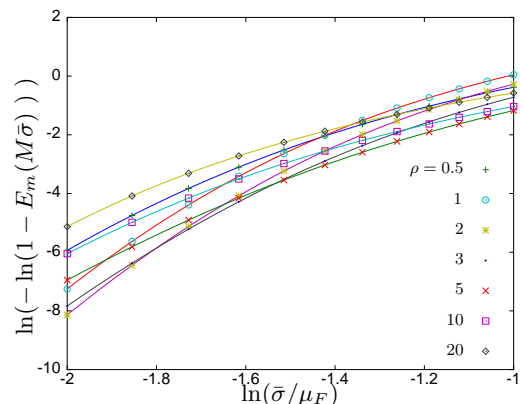


FIG. 16: (Colour online) Strength distribution of the m -fibre ELS bundles, for a range of ρ . The variation of m and M with ρ is given in Tab. I.

Based on Eqs. (16) and (18), $E_m(M\bar{\sigma})$ can be taken to represent the distribution of the elementary failure event underlying cluster growth in the present probabilistic model (Sec. III), approximately. Its distribution is plotted in Fig. 16. m and M vary with ρ as given in Tab. I. It is seen that $E_m(M\bar{\sigma})$ distributions are similar to each other for all ρ , in contrast to the fibre strength distributions, $\hat{F}(\sigma)$, shown in Fig. 4. This makes it plausible that cluster growth of ELS bundles to failure occurs for all ρ . If the elementary failure event were taken to be fibre failure, the same would not be true. For $\rho \geq 10$, whereat $m = 1$, the ELS bundle coincides with a fibre, the present model's elementary failure event coincides with that used in the literature [8, 10, 12], and the present probabilistic model coincides with the classical one [8, 10, 12]. For smaller ρ , however, the classical probabilistic models overestimate the failure probability, while the present model correctly estimates it.

Ibnabdeljalil and Curtin [13] and Curtin [14] were the first to suggest the link between LLS bundle failure and the failure of an ELS sub-bundle. Their scaling rules, Eqs. (6) and (7), assume that failure of an ELS bundle of a certain critical size, n_c represents the weakest-link event in the bundle failure. As shown in Sec. IV.3, this scaling rule breaks down for all ρ in the case of the present LLS bundle. ELS bundle failure is the elementary failure event in the present probabilistic model also. However, the role of the ELS bundles in the present model differs from that in Curtin [14] in the following significant ways: (i) The failure of the present m -bundle is but a part of the chain of events leading up to composite failure (Eq. (18)). The failure of any n_c bundle in Curtin [14] is the weakest-link event and implies composite failure. This also makes

the present m smaller than Curtin's [14] n_c for any given ρ . (ii) The present m -bundles experience stress concentrations from the failure of neighbouring m bundles and fail in response to these overloads. Local stress concentrations play no role in Curtin [14]. (iii) The present m -bundles may overlap, as shown in Fig. 3, and they do so for $\rho \leq 1$ (Table I). The n_c bundles in Curtin [14] do not.

Although there is no brittle-to-tough transition in the planar LLS bundle, a higher order transition appears to occur across $\rho = 1$. As seen from Tab. I, $p = 1$ for $\rho > 1$, but $p < 1$ for $\rho \leq 1$. As noted previously in Sec. III.3, $p = 1$ signifies the association of a weakest-link failure event with every fibre, while $p < 1$ signifies the same for every $(1/p)$ -th fibre. In LLS bundles with $\rho \leq 1$, the present results suggest that independent weakest-link events are not associated with each fibre, but with collections of $1/p$ fibres. No such transition is suggested by any of the foregoing probabilistic models.

VI. CONCLUSIONS

Using Monte-Carlo simulations and probabilistic modelling, the strength distribution of two dimensional local load sharing bundles with Weibull distributed fibre strengths and Poisson distributed fibre positions has been studied. The Monte-Carlo simulations show that the strength distribution has a weakest-link character for any Weibull exponent. A simple and accurate probabilistic model has been proposed for the bundle strength distributions. A key feature of the probabilistic model is the consideration of failure events at a size scale between that of a single fibre and that of the bundle, whose failure statistics follows that of equal load sharing bundles.

ACKNOWLEDGMENTS

The simulations were carried out at the High Performance Computing Environment at IIT Madras. We thank Prof. Ishan Sharma, IIT Kanpur for suggestions helpful in preparing the revised version of the manuscript.

-
- [1] M. J. Alava, P. K. Nukala, and S. Zapperi, *Adv. Phys.* **55**, 349 (2006).
 - [2] S. Pradhan, A. Hansen, and B. K. Chakrabarti, *Rev. Mod. Phys.* **82**, 499 (2010).
 - [3] H. Daniels, *Proc. R. Soc. Lond. A.* **183**, 405 (1945).
 - [4] J. M. Hedgepeth, *Stress concentrations in filamentary structures*, Tech. Rep. NASA-TN-D-882 (NASA, 1961).
 - [5] J. M. Hedgepeth and P. Van Dyke, *J. Compos. Mater.* **1**, 294 (1967).
 - [6] S. Mahesh, I. J. Beyerlein, and S. L. Phoenix, *Phys. D* **133**, 371 (1999).
 - [7] S. Mahesh, S. L. Phoenix, and I. J. Beyerlein, *Int. J. Fract.* **115**, 41 (2002).
 - [8] D. G. Harlow and S. L. Phoenix, *J. Compos. Mater.* **12**, 195 (1978).
 - [9] S. Phoenix and R. Smith, *Int. J. Solids Struct.* **19**, 479 (1983).
 - [10] R. Smith, S. Phoenix, M. Greenfield, R. Henstenburg, and R. Pitt, *Proc. R. Soc. Lond. A* **388**, 353 (1983).
 - [11] S. Mahesh and S. L. Phoenix, *Phys. Rev. E* **69**, 026102 (2004).
 - [12] R. L. Smith, *Proc. R. Soc. Lond. A* **372**, 539 (1980).
 - [13] M. Ibnabdeljalil and W. Curtin, *Int. J. Solids Struct.* **34**, 2649 (1997).
 - [14] W. Curtin, *Phys. Rev. Lett.* **80**, 1445 (1998).
 - [15] W. Weibull, *J. Appl. Mech* **103** (1951).
 - [16] S. Karlin and H. Taylor, *A First Course in Stochastic Processes* (Elsevier Science, 2012).
 - [17] W. Curtin, *J. Mech. Phys. Solids* **41**, 217 (1993).
 - [18] S. Zhou and W. Curtin, *Acta Metall. Mater.* **43**, 3093 (1995).
 - [19] I. J. Beyerlein, S. L. Phoenix, and A. M. Sastry, *Int. J. Solids Struct.* **33**, 2543 (1996).
 - [20] Z. Xia, W. Curtin, and P. Peters, *Acta Mater.* **49**, 273 (2001).
 - [21] Y. Swolfs, I. Verpoest, and L. Gorbatikh, *Compos. Sci. Tech.* **114**, 42 (2015).
 - [22] S. Torquato, *Random heterogeneous materials: microstructure and macroscopic properties*, Vol. 16 (Springer, 2013).
 - [23] F. Aurenhammer, *ACM Comput. Surv* **23**, 345 (1991).
 - [24] O. Devillers, *Int. J. Comp. Geom. Appl.* **12**, 193 (2002).
 - [25] P. Calka, *Adv. Appl. Probab.* **35**, 863 (2003).
 - [26] L. McCartney and R. Smith, *J. appl. mech.* **50**, 601 (1983).
 - [27] T. Kiang, *Z. Astrophys.* **64**, 433 (1966).